Crystal Growth

DOI: 10.1002/anie.200804528

Monodisperse BaF_2 Nanocrystals: Phases, Size Transitions, and Self-Assembly**

*Ting Xie, Shuai Li, Qing Peng, and Yadong Li**

Research on nanostructured materials and nanodevices is a rapidly growing field. Their development requires strict control and a deep understanding of the nucleation and growth mechanisms of nanocrystals,[1] as well as a way to modify[2] their morphologies during fabrication. Ideal individual nanocrystals are also required as building blocks for highly ordered superstructures.[3] Although a wide variety of nanocrystals with controllable sizes can be readily prepared and their superlattice assemblies obtained, the morphology evolution mechanism, especially the phase and size transition,[4] is not yet fully understood.[5] We believed BaF_2 nanocrystals to be a good model for investigation of the phase transition by thermodynamics[6] and the size transition by kinetics.[7]

Cubic-phase CaF_2 nanoparticles have been prepared by a hydrothermal approach without any surfactant.[8] Cubic-phase BaF_2 nanorods could be synthesized with the help of cetyltrimethylammonium bromide surfactant, which forms reverse micelles during the reaction.[9] However, to the best of our knowledge, reports on orthorhombic-phase BaF_2 are quite rare. Both cubic-phase and orthorhombic-phase BaF_2 are dielectric and have a wide range of potential applications in optoelectronics, since they have great optical-transmission domains and can be used as microelectronic devices, such as highly resistive dielectrics, wide-gap insulating layer, insulators, buffer layers, and solid-state ions.[10] BaF_2 doped with rare-earth ions has been reported to display unique luminescence properties and can be used as X-ray storage phosphors, scintillators,[11] as well as up- and down-conversion, and ionic conductivity materials. Recently, we reported a surface chemical thermodynamics (SCT) model to interpret the nucleation and growth of Ba_2F_3Cl nanorods under thermodynamic equilibrium.[12] In this study, the preparation of various BaF_2 nanocrystals was accomplished by the liquid–solid–solution (LSS) approach[13] with the products subsequently self-assembled by adding a buffer layer to the tube.[14] Herein, we report that the nucleation and growth of both cubic- and orthorhombic-phase BaF_2 crystals are under the control of nonequilibrium kinetics, whereas the phase transition of BaF_2 demonstrates that cubic-phase BaF_2 is thermodynamically stable. These two properties may shed light on the facile fabrication of various nanocrystals with controllable size and phase.

For the synthesis and self-assembly of monodisperse BaF_2 nanocrystals, uniform 5 ± 1 nm cubic-phase BaF_2 nanoparticles and 25 ± 1 nm orthorhombic-phase BaF_2 nanorods were prepared and self-assembled (Figure 1 a,b). The selected-area electron diffraction (SAED) patterns displayed in the insets of Figure 1 a,b also confirmed the complete self-assembly of BaF_2 nanocrystals, which should be distinguished from the partly assembled case (Figure S1 in the Supporting Information). In this process, the diffusion of methanol, a commonly used "nonsolvent" for precipitating nanocrystals, will disturb the system of oleic acid capped nanocrystals in cyclohexane. A buffer layer of propan-2-ol was then introduced between the nanocrystal solution and the methanol layer to slow down the precipitation of nanocrystals. Through this approach highly ordered self-assembly nanocrystals were formed at the interface of cyclohexane and the mixture. The HRTEM images (Figure 2 a,b) and powder XRD patterns (Figure 2 c,d) confirm the identification of cubic- and orthorhombic-phase BaF_2. Particularly, the XRD pattern of cubic-phase BaF_2 (Figure 2 c) shows several broad peaks because of their small sizes. Furthermore, EDS spectra (Figure S2 in the Supporting Information) confirm the high purity of the products.

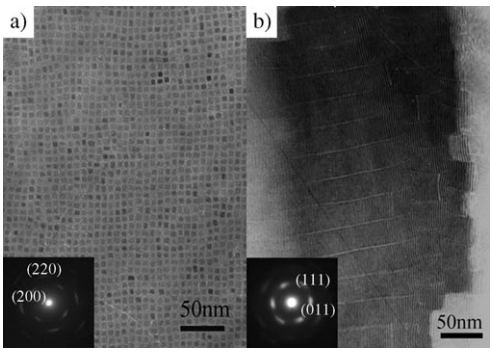

Figure 1. TEM images of the self-assembly of a) cubic- and b) orthorhombic-phase BaF_2 nanocrystals. The insets shows the SAED patterns.

Careful investigation of the TEM images in Figures 3 and 4 reveals that the BaF_2 nanocrystals underwent a remarkable size transition as the ripening time increased from 10 min to 48 h: the cubic-phase BaF_2 nucleated and grew from a) $4 \pm$

[*] T. Xie, S. Li, Dr. Q. Peng, Prof. Y. D. Li
Department of Chemistry, Tsinghua University
Beijing, 100084 (P.R. China)
Fax: (+86) 10-6278-8765
E-mail: ydli@tsinghua.edu.cn

[**] This work was supported by NSFC (90606006), the State Key Project of Fundamental Research for Nanoscience and Nanotechnology (2006CB932300), and the Key Grant Project of the Chinese Ministry of Education (No. 306020).

Supporting information for this article is available on the WWW under http://dx.doi.org/10.1002/anie.200804528.

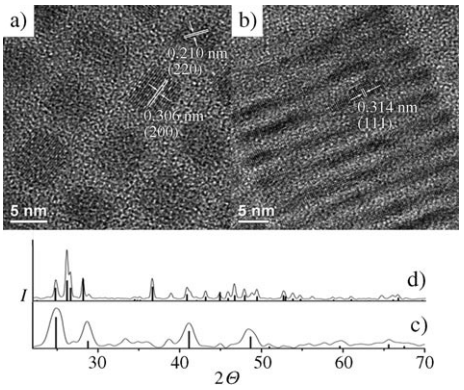

Figure 2. Typical HRTEM images of the a) cubic- and b) orthorhombic-phase BaF_2. Powder XRD patterns of c) cubic-phase (JCPDS card no. 85-1342) and d) orthorhombic-phase BaF_2 (JCPDS card no. 34-0200).

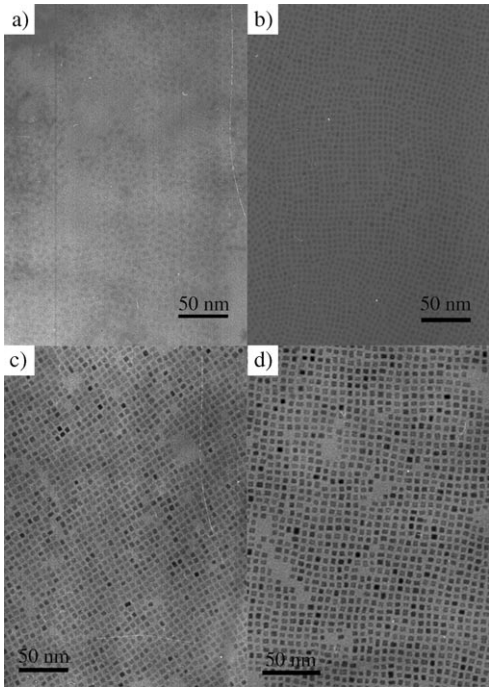

Figure 3. TEM images showing the nucleation and growth of cubic-phase BaF_2 for ripening times of a) 10 min, b) 12 h, c) 24 h, and d) 48 h.

1 nm spherical nanoparticles to b) 4 ± 1 nm truncated-square nanoparticles, then to c) 5 ± 1 nm complete-square nanoparticles, and finally to d) (5 ± 1) nm $\times$ (6 ± 1) nm rectangular nanoparticles (Figure 3); the TEM images in Figure 4 illustrate that the orthorhombic-phase BaF_2 underwent 1D growth from about 5 ± 0.5 nm long to 25 ± 1 nm, 50 ± 5 nm, and finally more than 300 nm, while the diameters only increased from 1.5 ± 0.1 nm to 3.5 ± 0.2 nm. Since the above growth process took place under nonequilibrium conditions, we applied a diffusion-controlled kinetic (DCK) model to explore the morphology evolution of both cubic- and orthorhombic-phase BaF_2 nanocrystals qualitatively. According to Wei and co-workers,[7] the reaction rates of BaF_2 monomers in our experiments are given by Equations (1a,b)

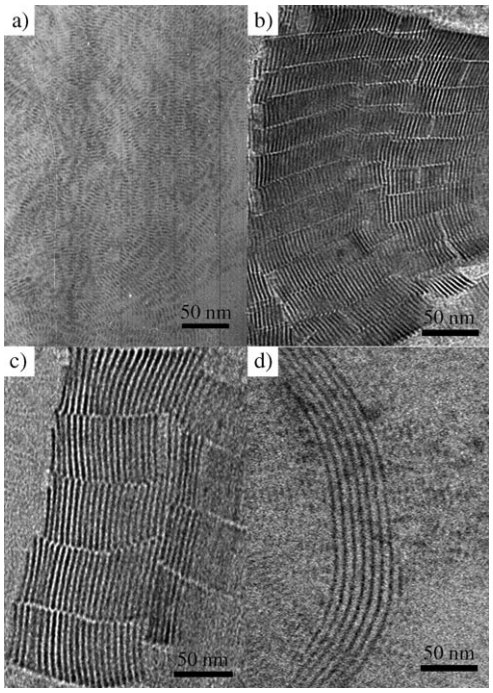

Figure 4. TEM images showing the nucleation and growth of orthorhombic-phase BaF_2 for ripening times of a) 10 min, b) 4 h, c) 8 h, and d) 12 h.

$$\nu_1 = D_1 s_1 R_{\text{eff}}^{-1} [n][A]^{a_1} \quad (1a)$$

$$\nu_2 = D_2 s_2 R_{\text{eff}}^{-1} [n][A]^{a_2} \quad (1b)$$

(see the Supporting Information), in which, the subscripts 1 and 2 represent the longitudinal and radial direction, respectively; D_1 and D_2 are diffusion coefficients; s_1 and s_2 are the corresponding surface areas; R_{eff} is the effective radius, as defined in Equation (S9) in the Supporting Information; [A] is the BaF_2 monomer concentration; $[n]$ is the concentration of the nanocrystals; and a_1 and a_2 are the order of the reactions. If g_r is the growth rate, then Equation (2) follows, in

$$g_r S_r = \nu_r V V_m \quad (2)$$

which V is the volume of reaction system; V_m is the molar volume of the solid nanocrystal; S_r is the sum of surface area "r" of all nanocrystals. Combining Equations (1a,b) and (2) gives Equations (3a,b), in which a_1, a_2, K_1, K_2 are constants,

$$g_1 = D_1 V_m R_{\text{eff}}^{-1} [A]^{a_1} = K_1 [A]^{a_1} \quad (3a)$$

$$g_2 = D_2 V_m R_{\text{eff}}^{-1} [A]^{a_2} = K_2 [A]^{a_2} \quad (3b)$$

and can be set as $a_1 = 1$, $a_2 = 2$, $K_1 = 1$, $K_2 = 10$, which renders the growth rates of BaF_2 nanocrystals concentration-dependent. How the morphology of a nanocrystal evolves can be simulated by solving the following time-related Equations (4a,b), in which L_1 and L_2 are the longitudinal and side

$$L_1(t + \Delta t) = L_1(t) + g_1 \Delta t \quad (4a)$$

$$L_2(t + \Delta t) = L_2(t) + g_2 \Delta t \quad (4b)$$

lengths. Since ΔL_1 and ΔL_2 of orthorhombic-phase BaF_2 nanorods are approximately constant according to our experiments (Figure 4a–c), while Δt is set 4 h to go along with the ripening time step, it can be drawn from Equations (4a,b) that g_1 and g_2 are time-independent. (Figure 4d is excluded because these nanowires are of various lengths, as seen from large-scale TEM images in Figure S3.) Thus, according to Equations (3a,b), the BaF_2 monomer concentration [A] is constant with time. An explanation to this phenomenon is that the growth process of orthorhombic-phase BaF_2 nanorods is marked by Ostwald ripening (OR): small crystals redissolve while larger crystals grow by consumption of the solute species; thus, the overall BaF_2 monomer concentration is a constant. The same DCK model and OR mechanisms apply well to cubic-phase BaF_2 nanoparticles (Figure 3).

To simplify this model we then introduce the relative growth rates of BaF_2 nanocrystals in length and radial directions [Eq. (5a,b)].

$$G_1 = g_1/L_1 \tag{5a}$$

$$G_2 = g_2/L_2 \tag{5b}$$

Since the initial concentration of Ba^{2+} is relatively high ($0.15\ mol\,L^{-1}$) for cubic-phase BaF_2 nanocrystals, it can be inferred from Equation (3) that $g_1 < g_2$, which means $G_1 < G_2$. Thus, the BaF_2 nucleus undergoes 3D growth and forms complete cubic-phase BaF_2 nanoparticles by Ostwald ripening. For orthorhombic-phase BaF_2, $g_1 > g_2$ because of the low value of [A] ($0.015\ mol\,L^{-1}$). Then, $G_1 > G_2$ and 1D growth is predominant, which leads to $L_1 > L_2$.

Furthermore, the size transition also depends greatly on the concentration of the oleic oil surfactant (Figure 5a,c). Similarly, the difference between Figures 5b and 5d can also be attributed to the surfactant effect. Compared with those in Figure 5c, the BaF_2 nanosheets in Figure 5a are much smaller and more regular; that is, without oleic acid, the cubic-phase BaF_2 grew much bigger in a more irregular way (Figure 5c), since the oleic acid was capped to the BaF_2 nanocores by strong chemical interactions, which blocked their further growth.

A number of experiments have shown that the synthesis of BaF_2 nanocrystals often results in orthorhombic-phase BaF_2 nanorods, which then easily transform into cubic-phase BaF_2 nanoparticles or nanosheets under certain conditions, especially at high reaction temperatures. It can be deduced statistically from our experimental results that a phase transition from orthorhombic- to cubic-phase BaF_2 nanocrystals occurred as a function of the ripening time and temperature (Figure 6c): at 140 °C, the resulting nanocrystals were pure orthorhombic-phase BaF_2; at 160 °C, a phase transition from orthorhombic- to cubic-phase BaF_2 began to occur as the ripening time reached 12 h;

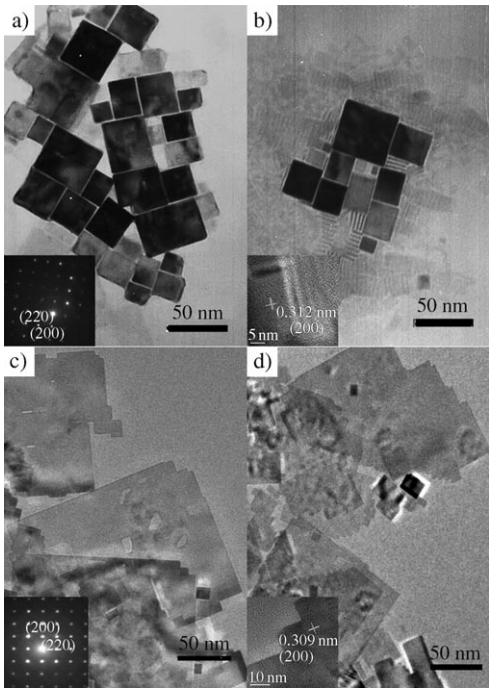

Figure 5. TEM images showing the shape and size transition of cubic-phase BaF_2 (a,c) and the phase transition from orthorhombic- to cubic-phase BaF_2 (b,d) for solvent including (a,b) and in the absence of oleic acid (c,d).

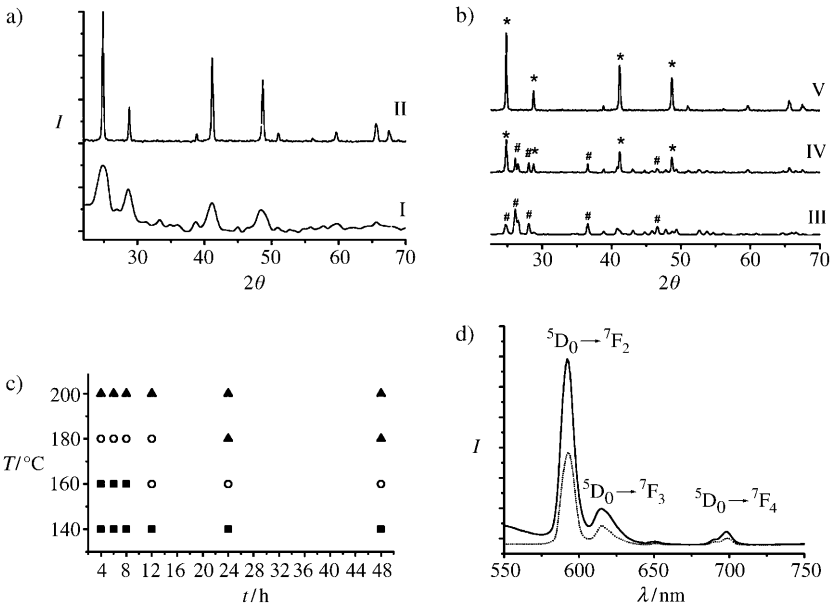

Figure 6. XRD data used to investigate a) the shape and size transition of cubic-phase BaF_2 and b) the phase transition from orthorhombic- to cubic-phase BaF_2. ⋆ cubic phase; # orthorhombic phase. I–V denote XRD patterns of I) small cubic-phase BaF_2 nanoparticles, II) large cubic-phase BaF_2 nanosheets, III) pure orthorhombic-phase BaF_2 nanocrystals, IV) mixed cubic- and orthorhombic-phase BaF_2, and V) pure cubic-phase BaF_2. c) The dependence of the BaF_2 phase on ripening time and temperature. ▲ cubic, ○ orthorhombic and cubic, ■ orthorhombic. d) Room-temperature fluorescence spectra of as-prepared cubic-phase (——) and orthorhombic-phase (----) BaF_2 nanocrystals doped with 5% Eu^{3+}.

at 180 °C, the phase transition started from the very beginning and ended up with neat cubic-phase BaF_2 as the ripening time exceeded 24 h; at 200 °C, only cubic-phase BaF_2 was produced no matter how long the reaction lasted. Moreover, it can be seen clearly from Figure 5b that the orthorhombic BaF_2 nanorods lay in an ordered arrangement along four sides of the cubic phase BaF_2 nanosheets. We can infer from this phenomenon that under such conditions the orthorhombic BaF_2 nanorods easily aggregated and transformed into cubic-phase BaF_2 nanosheets. Herein, the phase transition was investigated by using thermodynamics, in which phase stability played a crucial role. The orthorhombic-phase BaF_2 nanocrystals were stable only at relatively low reaction temperatures but became unsteady with the increase of temperature, while the cubic-phase nanocrystalline BaF_2 were more thermodynamically stable at high temperatures. So at relatively low temperatures, for example, 140–160 °C, we obtained orthorhombic-phase BaF_2 nanocrystals. However, as the temperature was increased to 180 °C, the orthorhombic-phase nanocrystalline BaF_2 became volatile and changed into cubic-phase BaF_2 nanosheets, which can stand high temperatures. XRD data can be used to investigate the size transition of cubic-phase BaF_2 (Figure 6a) and the phase transition from orthorhombic- to cubic-phase BaF_2 (Figure 6b). Moreover, many experiments have justified that nanocrystalline BaF_2 phase can be a key factor responsible for their optical properties. Room-temperature fluorescence spectra of the as-prepared BaF_2 nanocrystals doped with 5% Eu^{3+} show that the photoluminescence of cubic-phase BaF_2 (Figure 6d, solid curve) is at least twice as strong as that of orthorhombic-phase BaF_2 (Figure 6d, dashed curve).

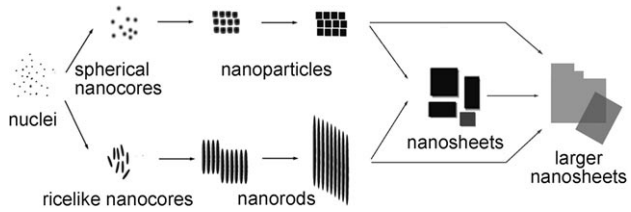

Figure 7. Procedure illustrating the formation and morphology evolution of cubic-phase and orthorhombic-phase BaF_2.

Figure 7 shows a schematic diagram of the nucleation and growth mechanism of BaF_2 nanocrystals. BaF_2 nuclei can be easily obtained under suitable synthetic conditions. Then, the spherical BaF_2 nanocores underwent 3D growth as the ripening time was extended and formed cubic-phase BaF_2 nanosheets through OR at relatively high reaction temperatures (Figure 7, top route); at low temperatures, the rice-like BaF_2 nanocores underwent 1D growth and ripened into rodlike orthorhombic-phase BaF_2, which was stable only under low reaction temperatures (Figure 7, bottom route). With increasing ripening time, orthorhombic BaF_2 nanorods grew longer through OR and transformed into cubic-phase BaF_2 nanosheets at 180 °C or above, and finally into large irregular nanosheets in the absence of oleic acid. The surfactant (oleic acid) played a significant role in this process: without oleic acid the BaF_2 nanosheets grew much larger and more irregular. Larger irregular BaF_2 nanosheets can be obtained either by small BaF_2 nanosheets or directly from the as-obtained cubic BaF_2 nanoparticles and orthorhombic BaF_2 nanorods, which were centrifuged, purified, resuspended in ethanol/cyclohexane, and then heated in a 50 mL teflon-lined autoclave at 200 °C without oleic acid.

In conclusion, self-assembled cubic-phase and orthorhombic-phase BaF_2 nanocrystals were synthesized by LSS with ripening times varying from 10 min to 48 h. The size transition and morphology evolution of BaF_2 nanocrystals under non-equilibrium conditions were studied and interpreted by using a DCK model, in which the OR process was predominant. Furthermore, the phase transition from orthorhombic- to the more thermodynamically stable cubic-phase BaF_2 was investigated on the basis of thermodynamics. The nucleation and growth of nanocrystalline BaF_2, including their size and phase transitions, were studied in detail. The results may help in the control and manipulation of the shape and phase of various nanocrystals.

Experimental Section

All the chemicals were of analytical grade and used as received without further purification. In a typical procedure, an aqueous solution of barium salt was mixed with oleic acid (20 mL), NaOH (1.2 g), alcohol (10 mL), and then thoroughly stirred at room temperature for 5–10 min to form an even mixture. A white amorphous precipitate appeared immediately after adding aqueous HF (5 wt%) to this mixture. The colloidal solution was vigorously stirred for another 10 min, transferred into a 50 mL teflon-lined autoclave, sealed, and heated at 140–200 °C. Then, the system was allowed to cool to room temperature. The final product was collected, purified by centrifugation, and washed several times with ethanol and cyclohexane to remove surfactants.

For the preparation of cubic-phase BaF_2 nanoparticles (ca. 5 nm), the initial concentration of $BaCl_2$ was about 0.15 mol L^{-1} and 40 wt% aqueous HF (0.75 mL) was used; the autoclaves were sealed and heated at 180 °C for 12–48 h. For the synthesis of orthorhombic BaF_2, $Ba(NO_3)_2$ was used as a precursor instead of $BaCl_2$ and its initial concentration was decreased to 0.015 mol L^{-1}, and a stoichiometric proportion of HF was used; the autoclaves were heated at 160 °C for 4–12 h. The above fabricating approach adopted the LSS synthetic strategy reported by our group.[13] The as-obtained BaF_2 nanocrystals were then self-assembled into highly ordered assemblies.[14]

The phase purity and crystallinity of the products were detected by XRD analysis on a Brucker D8-advance X-ray diffractometer with $Cu_{K\alpha}$ radiation ($\lambda = 1.5418$ Å), and the operating voltage and current were kept at 40 kV and 40 mA, respectively. The size and morphology of the products were observed by using the JEOL JEM-1200EX transmission electron microscope (TEM) with a tungsten filament working at 100 kV. Samples were directly transferred to a carbon-coated copper support grid for TEM, by adding dropwise a dilute cyclohexane dispersion of the nanocrystals on the surface of a copper grid. High-resolution transmission electron microscopy (HRTEM) images were obtained on a JEOL JEM-2010F transmission electron microscope. EDS was also performed to determine the elements of the products.

Received: September 15, 2008
Revised: October 7, 2008
Published online: December 3, 2008

Keywords: crystal engineering · kinetics · nanostructures · phase transitions · self-assembly

[1] a) C. B. Murray, D. J. Norris, M. G. Bawendi, *J. Am. Chem. Soc.* **1993**, *115*, 8706 – 8715; b) A. P. Alivisatos, *Science* **1996**, *271*, 933 – 937; c) X. G. Peng, L. Manna, W. D. Yang, J. Wickham, E. Scher, A. Kadavanich, A. P. Alivisatos, *Nature* **2000**, *404*, 59 – 61; d) Z. A. Peng, X. G. Peng, *J. Am. Chem. Soc.* **2001**, *123*, 1389 – 1395; e) R. Viswanatha, D. M. Battaglia, M. E. Curtis, T. D. Mishima, M. B. Johnson, X. G. Peng, *Nano Res.* **2008**, *1*, 138 – 144.

[2] a) L. Y. Wang, R. X. Yan, Z. Y. Huo, et al., *Angew. Chem.* **2005**, *117*, 6208 – 6211; *Angew. Chem. Int. Ed.* **2005**, *44*, 6054 – 6057; b) X. M. Sun, Z. Liu, K. Welsher, J. T. Robinson, A. Goodwin, S. Zaric, H. J. Dai, *Nano Res.* **2008**, *1*, 203 – 212.

[3] a) J. E. Bowen Katari, V. L. Colvin, A. P. Alivisatos, *J. Phys. Chem.* **1994**, *98*, 4109; b) C. B. Murray, C. R. Kagan, M. G. Bawendi, *Science* **1995**, *270*, 1335 – 1338; c) M. Li, H. Schnablegger, S. Mann, *Nature* **1999**, *402*, 393; d) E. V. Shevchenko, D. V. Talapin, N. A. Kotov, S. O'Brien, C. B. Murray, *Nature* **2006**, *439*, 55 – 59; e) F. Bai, D. S. Wang, Z. Y. Huo, et al., *Angew. Chem.* **2007**, *119*, 6770 – 6773; *Angew. Chem. Int. Ed.* **2007**, *46*, 6650 – 6653; f) Z. B. Zhuang, Q. Peng, X. Wang, Y. D. Li, *Angew. Chem.* **2007**, *119*, 8322 – 8325; *Angew. Chem. Int. Ed.* **2007**, *46*, 8174 – 8177.

[4] A. S. Barnard, L. A. Curtiss, *Nano Lett.* **2005**, *5*, 1261 – 1266.

[5] S. Kumar, T. Nann, *Small* **2006**, *2*, 316 – 329.

[6] L. Manna, L. W. Wang, R. Cingolani, A. P. Alivisatos, *J. Phys. Chem. B* **2005**, *109*, 6183 – 6192.

[7] X. X. Xu, F. Liu, K. Yu, W. Huang, B. Peng, W. Wei, *ChemPhysChem* **2007**, *8*, 703 – 711.

[8] X. M. Sun, Y. D. Li, *Chem. Commun.* **2003**, *14*, 1768 – 1769.

[9] a) M. H. Cao, C. W. Hu, E. B. Wang, *J. Am. Chem. Soc.* **2003**, *125*, 11196 – 11197; b) R. N. Hua, C. Y. Zang, C. Sha, D. M. Xie, C. S. Shi, *Nanotechnology* **2003**, *14*, 588 – 591; c) P. Gao, Y. Xie, Z. Li, *Eur. J. Inorg. Chem.* **2006**, *16*, 3261 – 3265; d) G. H. De, W. P. Qin, J. Zhang, J. H. Zhang, Y. Wang, C. Y. Cao, Y. Cui, *J. Solid State Chem.* **2006**, *179*, 955 – 958; e) X. M. Zhang, Z. W. Quan, J. Yang, P. P. Yang, H. Z. Lian, J. Lin, *Nanotechnology* **2008**, *19*, 075603.

[10] M. Kobayashi, *Solid State Ionics* **2004**, *174*, 57 – 66.

[11] A. J. Wojtowicz, *Nucl. Instrum. Methods Phys. Res. Sect. A* **2002**, *486*, 201 – 207.

[12] T. Xie, S. Li, Q. Peng, Y. D. Li, *Chem. Eur. J.* **2008**, *14*, 9730.

[13] X. Wang, J. Zhuang, Q. Peng, Y. D. Li, *Nature* **2005**, *437*, 121 – 124.

[14] D. V. Talapin, E. V. Shevchenko, A. Kornowski, N. Gaponik, M. Haase, A. L. Rogach, H. Weller, *Adv. Mater.* **2001**, *13*, 1868.

